Journal of Dental Research
2021, Vol. 100(9) 993–1001
© International & American Associations for Dental Research 2021
Article reuse guidelines:
sagepub.com/journals-permissions
DOI: 10.1177/00220345211005677
journals.sagepub.com/home/jdr

Delivery of Alkaline Phosphatase Promotes Periodontal Regeneration in Mice

A. Nagasaki[1], K. Nagasaki[1], B.D. Kear[1], W.D. Tadesse[1], V. Thumbigere-Math[2], J.L. Millán[3], B.L. Foster[4], and M.J. Somerman[1]

Abstract

Factors regulating the ratio of pyrophosphate (PP_i) to phosphate (P_i) modulate biomineralization. Tissue-nonspecific alkaline phosphatase (TNAP) is a key promineralization enzyme that hydrolyzes the potent mineralization inhibitor PP_i. The goal of this study was to determine whether TNAP could promote periodontal regeneration in bone sialoprotein knockout mice (*Ibsp*$^{-/-}$ mice), which are known to have a periodontal disease phenotype. Delivery of TNAP was accomplished either systemically (through a lentiviral construct expressing a mineral-targeted TNAP-D_{10} protein) or locally (through addition of recombinant human TNAP to a fenestration defect model). Systemic TNAP-D_{10} delivered by intramuscular injection at 5 d postnatal (dpn) increased circulating alkaline phosphatase (ALP) levels in *Ibsp*$^{-/-}$ mice by 5-fold at 30 dpn, with levels returning to normal by 60 dpn when tissues were evaluated by micro–computed tomography and histology. Local delivery of recombinant human TNAP to fenestration defects in 5-wk-old wild type (WT) and *Ibsp*$^{-/-}$ mice did not alter long-term circulating ALP levels, and tissues were evaluated by micro–computed tomography and histology at postoperative day 45. Systemic and local delivery of TNAP significantly increased alveolar bone volume (20% and 37%, respectively) and cementum thickness (3- and 42-fold) in *Ibsp*$^{-/-}$ mice, with evidence for periodontal ligament attachment and bone/cementum marker localization. Local delivery significantly increased regenerated cementum and bone in WT mice. Addition of 100-μg/mL bovine intestinal ALP to culture media to increase ALP in vitro increased media P_i concentration, mineralization, and *Spp1* and *Dmp1* marker gene expression in WT and *Ibsp*$^{-/-}$ OCCM.30 cementoblasts. Use of phosphonoformic acid, a nonspecific inhibitor of sodium P_i cotransport, indicated that effects of bovine intestinal ALP on mineralization and marker gene expression were in part through P_i transport. These findings show for the first time through multiple in vivo and in vitro approaches that pharmacologic modulation of P_i/PP_i metabolism can overcome periodontal breakdown and accomplish regeneration.

Keywords: biomineralization, cementogenesis, bone regeneration, periodontium, extracellular matrix, phosphates

Introduction

Periodontal disease causes destruction of cementum, periodontal ligament (PDL), and surrounding alveolar bone. Approximately 45% of US adults suffer from periodontal disease that, when left untreated, can result in tooth loss (Eke et al. 2016). The goals of periodontal therapy are to eliminate pathogenic microbes, resolve inflammation, and restore periodontal structure and function; however, current therapies are often suboptimal (Foster et al. 2007; Sallum et al. 2019). This is particularly true for cementum, a tissue with limited capacity for repair.

Identification of therapeutic approaches inspired by understanding the developmental biology of periodontal tissues may lead to improved therapeutic outcomes. Studies from our group and others revealed that appropriate balance in levels of inorganic phosphate (P_i), a promoter of hydroxyapatite formation, and pyrophosphate (PP_i), a potent inhibitor of hydroxyapatite crystal growth, is crucial for proper mineralization and that acellular cementum is particularly sensitive to this mechanism of regulation (Foster et al. 2012; Ao et al. 2017; Thumbigere-Math et al. 2018; Chu et al. 2020; Nagasaki et al. 2020). Three P_i/PP_i regulators work in concert to direct mineralization of periodontal tissues. Tissue-nonspecific alkaline phosphatase (gene: *Alpl*, mouse; *ALPL*, human; protein: TNAP) promotes mineralization by hydrolyzing PP_i to produce P_i (Millan 2006). TNAP is expressed by mineralizing cells, including cementoblasts

[1]Laboratory of Oral Connective Tissue Biology, National Institute of Arthritis and Musculoskeletal and Skin Diseases, National Institutes of Health, Bethesda, MD, USA
[2]Division of Periodontology, School of Dentistry, University of Maryland, Baltimore, MD, USA
[3]Sanford Burnham Prebys Medical Discovery Institute, La Jolla, CA, USA
[4]Biosciences Division, College of Dentistry, The Ohio State University, Columbus, OH, USA

A supplemental appendix to this article is available online.

Corresponding Author:
A. Nagasaki, Laboratory of Oral Connective Tissue Biology, National Institute of Arthritis and Musculoskeletal and Skin Diseases, National Institutes of Health, 9000 Rockville Pike, Building 50, Room 4120, Bethesda, MD 20892, USA.
Email: atsuhiro.nagasaki@nih.gov

and osteoblasts, and loss-of-function mutations result in increased PP_i levels and the inherited hypomineralization disorder hypophosphatasia (HPP; OMIM#241500, 241510, 146300), which features tooth loss due to cementum defects (Bowden and Foster 2019). The progressive ankylosis protein (*Ank*/ANK in mouse, *ANKH*/ANK in human) is a transmembrane regulator of PP_i transport to the extracellular space (Ho et al. 2000; Szeri et al. 2020). Ectonucleotide pyrophosphatase phosphodiesterase 1 (*Enpp1*/ENPP1) is an ectoenzyme that extracellularly cleaves nucleotide triphosphates to PP_i (Rutsch et al. 2003). ANK and ENPP1 increase local PP_i levels, and loss of function of either gene causes PP_i deficiency and hypermineralization disorders—that is, ectopic calcification: generalized arterial calcification in infancy (OMIM# 208000) and craniometaphyseal dysplasia (OMIM# 123000), respectively. Loss of ANK or ENPP1 results in dramatically thicker acellular cementum in mice, and similarly expanded acellular cementum results from generalized arterial calcification in infancy in humans (Foster et al. 2012; Dutra et al. 2013; Zweifler et al. 2015; Ao et al. 2017; Thumbigere-Math et al. 2018; Chu et al. 2020). We reported that genetic reduction of PP_i by crossing *Ank*$^{-/-}$ mice with *Alpl*$^{-/-}$ mice corrected cementum developmental defects (Chu et al. 2020). Furthermore, loss of ANK or ENPP1 promotes cementum regeneration in a periodontal fenestration model (Rodrigues et al. 2011; Nagasaki et al. 2020), implicating modifiers of P_i/PP_i metabolism as strategies to promote periodontal regeneration.

Mice lacking bone sialoprotein (*Ibsp*/BSP), an extracellular matrix (ECM) protein, exhibit severe periodontal breakdown, including reduced cementum, PDL disorganization, and alveolar bone destruction (Foster et al. 2013; Foster et al. 2015). Genetic reduction of PP_i by crossing *Ank*$^{-/-}$ with *Ibsp*$^{-/-}$ mice resulted in correction of cementum defects noted in *Ibsp*$^{-/-}$ mice (Ao et al. 2017). We aimed to build on these findings by determining if pharmacologic approaches to decrease PP_i and increase P_i levels through delivery of TNAP could correct cementum defects and promote cementum regeneration in *Ibsp*$^{-/-}$ model of periodontal disease. We employed a lentivirus construct expressing mineral-targeted TNAP (Yamamoto et al. 2011) for systemic delivery to treat developmental defects in the *Ibsp*$^{-/-}$ model. We used recombinant human TNAP (rhTNAP) for local delivery to treat periodontal fenestration defects (Rodrigues et al. 2011) in adult *Ibsp*$^{-/-}$ mice. An *Ibsp*$^{-/-}$ cementoblast cell line was used to determine effects of bovine intestinal alkaline phosphatase (bIAP) on gene expression and mineralization in vitro.

Materials and Methods

Animals

Animal procedures were conducted in accordance with the guidelines of the Animal Care and Use Committee, National Institutes of Health. *Ibsp*$^{-/-}$ mice on a mixed 129/CD1 background were described previously (Ao et al. 2017). Male wild type (WT) control and *Ibsp*$^{-/-}$ mice were employed to minimize potential sex-related variability. At weaning, mice were provided a soft diet (Diet Gel 31M; ClearH2O) in addition to normal chow (NIH-31) to reduce incisor malocclusion in *Ibsp*$^{-/-}$ mice.

Systemic TNAP Lentiviral Vector Delivery

A lentiviral vector expressing mineral-targeted TNAP with a deca-aspartate tail (TNAP-D_{10}) was prepared (Cellomics Technology; Yamamoto et al. 2011). Lentivirus (5.0×10^7 transduction units) was injected intramuscularly into 5-d-postnatal (dpn) *Ibsp*$^{-/-}$ mice, and phosphate buffered saline (PBS) vehicle was injected into control *Ibsp*$^{-/-}$ and WT mice ($n = 3$/genotype). Blood was collected at 30 and 60 dpn to measure plasma alkaline phosphatase (ALP) levels. Mice were euthanized at 60 dpn. Additional details are in the Appendix.

Local Recombinant Human TNAP Delivery

For local delivery of rhTNAP (0.1 µg in 1 µL; R&D Systems), a mouse fenestration defect model modified from previous reports was performed on WT and *Ibsp*$^{-/-}$ mice (King et al. 1997; Rodrigues et al. 2011). Five-week-old mice were selected by developmental stage of tooth root and mandibular bone; that is, root formation is complete, and the teeth are in occlusion (Appendix Fig. 1; Vora et al. 2016; Chu et al. 2020). PBS (1 µL) was used as negative control ($n = 6$/group). Blood was collected, and mice were euthanized on postoperative day 45 (POD 45). Additional details are provided in the Appendix.

Micro–computed tomography

Hemimandibles fixed in 10% neutral buffered formalin were scanned in 70% ethanol in a µCT 50 (Scanco Medical) as reported (Ao et al. 2017). Reconstructed images were analyzed with AnalyzePro (version 1.0; AnalyzeDirect). Additional details are in the Appendix.

Histology

Tissues were decalcified in a solution of acetic acid, formalin, and sodium chloride and paraffin embedded for 5-µm sections (Ao et al. 2017). Hematoxylin and eosin staining, immunohistochemistry, picrosirius red staining, and histomorphometry are described in the Appendix.

Cell Culture

Ibsp$^{-/-}$ OCCM.30 immortalized murine cementoblasts were engineered with CRISPR/Cas9 (Ao et al. 2017). *Ibsp*$^{-/-}$ and WT cells were maintained in Dulbecco's modified Eagle's medium (Life Technologies Corporation) with 10% fetal bovine serum (Hyclone Laboratories) and induced to promote mineral nodule formation in mineralization media: 2% fetal bovine serum, 50-µg/mL ascorbic acid (Sigma-Aldrich), and

10mM β-glycerophosphate (Sigma-Aldrich). bIAP (Sigma-Aldrich) at 100 µg/mL was used to increase phosphatase activity (Osathanon et al. 2009), and phosphonoformic acid (PFA; Sigma-Aldrich) was used to inhibit sodium phosphate cotransport (Foster et al. 2012). Media P_i levels were analyzed following manufacturer's directions (Sigma-Aldrich). Mineralization was measured by alizarin red stain (EMS) as previously described (Foster et al. 2012). Additional details are in the Appendix.

Quantitative Polymerase Chain Reaction

Quantitative polymerase chain reaction was performed on RNA from cells as detailed in the Appendix, with primer sequences listed in the Appendix Table.

Statistical Analysis

Results are reported as mean ± SD. Data were analyzed (Prism 7; GraphPad Software) by independent samples *t* test where $*P < 0.05$, $**P < 0.01$, or $***P < 0.001$ indicate significance, or by 1-way ANOVA with post hoc Tukey test, where experimental groups marked by different letters are significantly different ($P < 0.05$) and groups sharing the same letter are not different ($P > 0.05$).

Results

Systemic TNAP-D_{10} Delivery Improves Periodontal Development in Ibsp$^{-/-}$ *Mice*

To determine whether systemic delivery of TNAP could overcome cementum defects in *Ibsp*$^{-/-}$ mice, mice at 5 dpn (prior to molar root formation) were injected intramuscularly with lentivirus encoding mineral-targeted TNAP-D_{10}. TNAP-D_{10} increased plasma ALP nearly 5-fold versus PBS WT and *Ibsp*$^{-/-}$ mice at 30 dpn, with return to normal levels by 60 dpn (Fig. 1A).

Cementum and PDL were evaluated by histology. At 60 dpn, TNAP-D_{10} increased buccal and lingual cementum thickness versus vehicle-treated *Ibsp*$^{-/-}$ mice (3- and 2-fold, respectively), though cementum thickness remained 20% to 40% reduced when compared with WT (Fig. 1B). By hematoxylin and eosin stain, vehicle-treated *Ibsp*$^{-/-}$ mice exhibited detached, disorganized PDL. TNAP-D_{10} reestablished PDL attachment and organization comparable to that of untreated control WT mice (Fig. 1C). The restored cementum was immunostained for ECM markers osteopontin (OPN) and dentin matrix protein 1 (DMP1). Vehicle-treated *Ibsp*$^{-/-}$ mice lacked clear OPN localization indicative of the root surface acellular cementum seen in WT controls (Fig. 1D). TNAP-D_{10} increased OPN deposition on *Ibsp*$^{-/-}$ mouse root surfaces. In contrast to minimal DMP1 expression in the cementum of PBS *Ibsp*$^{-/-}$ and untreated control WT mice, TNAP-D_{10} increased DMP1 expression along the root surface (Fig. 1E). Asporin (*Aspn*/

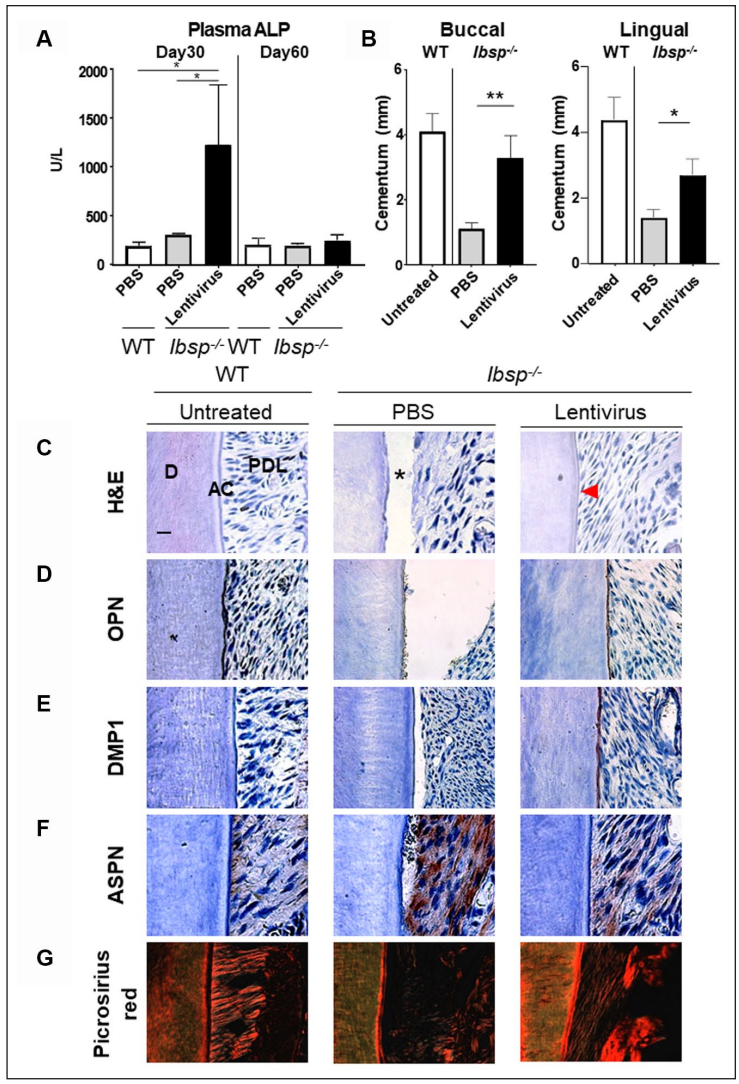

Figure 1. Systemic delivery of TNAP-D_{10} restores cementum formation in *Ibsp*$^{-/-}$ mice. Mice at 5 d postnatal (dpn) were injected intramuscularly with TNAP-D_{10} lentiviral vector or phosphate-buffered saline (PBS) vehicle and evaluated at 60 dpn. (**A**) TNAP-D_{10} increases plasma alkaline phosphatase (ALP) levels by 5-fold over PBS vehicle at 30 dpn, with no persistent differences at 60 dpn ($n = 3$ mice/group; $*P < 0.05$, by 1-way analysis of variance). (**B**) When compared with PBS vehicle, TNAP-D_{10} treatment significantly increased buccal and lingual acellular cementum (AC) thickness in *Ibsp*$^{-/-}$ mice (3- and 2-fold, respectively) at 60 dpn, though cementum thickness remained less than that of wild type (WT) mice ($n = 3$ mice/group; $*P < 0.05$, $**P < 0.01$ by *t* test). Values are presented as mean ± SD. (**C**) Hematoxylin and eosin (H&E) staining reveals lack of AC on root dentin (D) and detachment of the periodontal ligament (PDL) from root surfaces (*) in vehicle-treated *Ibsp*$^{-/-}$ mice. TNAP-D_{10} reestablishes AC and PDL attachment (arrowhead) in *Ibsp*$^{-/-}$ mice. (**D**) Unlike robust osteopontin (OPN) in AC of untreated control WT mice, PBS-treated *Ibsp*$^{-/-}$ mice lack OPN localization on root surfaces. TNAP-D_{10} restores OPN on *Ibsp*$^{-/-}$ mouse root surfaces. (**E**) In contrast to minimal dentin matrix protein 1 (DMP1) localization in AC of WT and PBS-treated *Ibsp*$^{-/-}$ mice, TNAP-D_{10} increases DMP1 localization along root surfaces. (**F**) When compared with WT, *Ibsp*$^{-/-}$ mice exhibit robust localization of ASPN in root-associated PDL. TNAP-D_{10} treatment reduces ASPN in *Ibsp*$^{-/-}$ mouse PDL. (**G**) Picrosirius red staining revealed that TNAP-D_{10} induced PDL attachment in *Ibsp*$^{-/-}$ mice. Representative images from 3 mice. Scale bar: 20 µm.

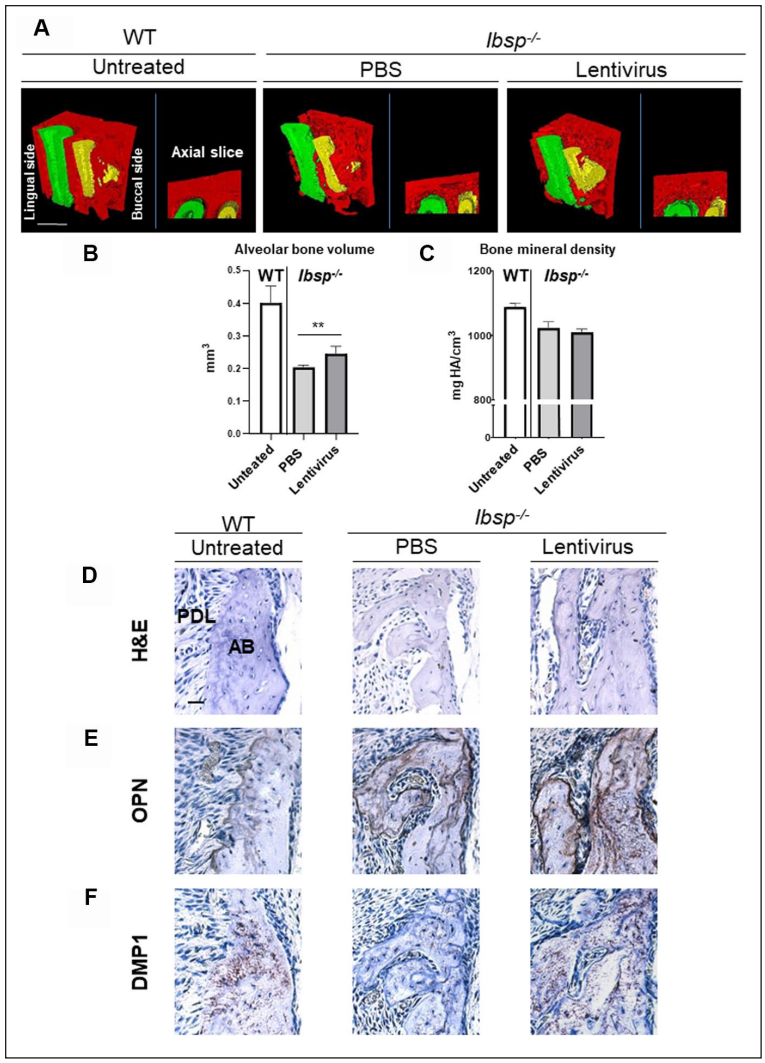

Figure 2. Increased alveolar bone volume in *Ibsp*$^{-/-}$ mice from systemic delivery of TNAP-D_{10}. Mice at 5 d postnatal (dpn) were injected intramuscularly injected with TNAP-D_{10} lentiviral vector or phosphate-buffered saline (PBS) vehicle and evaluated at 60 dpn. (**A**) Three-dimensional micro–computed tomography renderings of first mandibular molar distal (green) and second molar mesial (yellow) roots and surrounding alveolar bone (AB; red). Scale bar: 500 μm. (**B**) TNAP-D_{10} significantly increases alveolar bone volume by 20% in *Ibsp*$^{-/-}$ mice, (**C**) though alveolar bone density was not altered ($n = 3$ mice; $^{**}P < 0.01$ by t test). Values are presented as mean ± SD. (**D**) Hematoxylin and eosin (H&E) staining reveals improved AB formation in TNAP-D_{10} versus untreated *Ibsp*$^{-/-}$ mice. (**E**) Immunohistochemistry indicates more robust osteopontin (OPN) localization in AB of *Ibsp*$^{-/-}$ versus wild type (WT) mice, with additional OPN associated with TNAP-D_{10} treatment. (**F**) TNAP-D_{10} restores normal distribution of dentin matrix protein 1 (DMP1) in AB of *Ibsp*$^{-/-}$ mice. Scale bar: 25 μm.

ASPN), suggested to be a negative regulator of mineralization (Yamada et al. 2007; Kajikawa et al. 2014), was increased in the PDL of *Ibsp*$^{-/-}$ versus untreated control WT mice (Fig. 1F). TNAP-D_{10} reduced ASPN in *Ibsp*$^{-/-}$ mice to levels approaching normal. Picrosirius red staining revealed that TNAP-D_{10} induced PDL attachment onto the root surfaces of *Ibsp*$^{-/-}$ mice, although organization differed from WT mice (Fig. 1G).

Alveolar bone was evaluated by micro–computed tomography and histology. Alveolar bone volume increased 20% in TNAP-D_{10} treated versus untreated *Ibsp*$^{-/-}$ mice, though volumes remained reduced versus untreated control WT levels (Fig. 2A, B). Treatment did not significantly alter *Ibsp*$^{-/-}$ mouse alveolar bone density, which remained decreased versus control WT (Fig. 2C). Immunohistochemistry revealed intense OPN staining in *Ibsp*$^{-/-}$ versus untreated control WT alveolar bone, and additional OPN deposition was associated with TNAP-D_{10} treatment in *Ibsp*$^{-/-}$ mice (Fig. 2E). TNAP-D_{10} also restored DMP1 expression in alveolar bone of *Ibsp*$^{-/-}$ mice to levels comparable to those of WT mice (Fig. 2F).

Local Delivery of rhTNAP Promotes Cementum and Alveolar Bone Regeneration in Ibsp$^{-/-}$ *Mice*

Because systemic delivery of TNAP-D_{10} restored cementogenesis and periodontal structures in *Ibsp*$^{-/-}$ mice, supporting the concept that pharmacologic modulation of P_i/PP_i can overcome inherent mineralization defects, we next determined the efficacy of local rhTNAP delivery, a more realistic translational approach amenable to clinical treatment of periodontal disease. Fenestration defects were created in 5-wk-old mice. The POD 45 recovery period was uneventful, with no overt signs of inflammation or infection. There were no significant differences among groups in plasma ALP levels at POD 45 (Fig. 3A).

Cementum and PDL were evaluated by histology. rhTNAP increased cementum thickness in WT mice and promoted formation of a cementum-like layer on the root surfaces of *Ibsp*$^{-/-}$ mice (21- and 42-fold, respectively), with mineralized matrix extending into the PDL space, though tooth-bone ankylosis was not observed (Fig. 3B, C). rhTNAP improved cementum-PDL attachment as compared with vehicle-treated *Ibsp*$^{-/-}$ mice (Fig. 3C). Localization of OPN and DMP1 on *Ibsp*$^{-/-}$ mouse root surfaces was observed in response to rhTNAP, though treatment differences were not apparent in WT mice, suggesting more active, ongoing cementogenesis in tissues with inherently compromised cementum, for example, *Ibsp*$^{-/-}$ mice (Fig. 3D, E). ASPN localization in PDL appeared less intense in rhTNAP *Ibsp*$^{-/-}$ mice versus vehicle controls (Fig. 3F). Local rhTNAP delivery induction of PDL attachment in *Ibsp*$^{-/-}$ mice was confirmed by picrosirius red staining (Fig. 3G). However, PDL organization in all experimental groups was reduced when compared with unoperated WT mice (Appendix Fig. 2), suggesting limitations of the study approach and/or time frame.

Alveolar bone was evaluated by micro–computed tomography and histology. rhTNAP significantly increased alveolar bone volume and density in WT (17% and 5%, respectively)

and *Ibsp*$^{-/-}$ mice (37% and 5%; Fig. 4A–C). Local rhTNAP delivery restored localization of OPN and DMP1 to regenerated alveolar bone of WT and *Ibsp*$^{-/-}$ mice (Fig. 4D, E).

bIAP Increases Mineralization in Cementoblasts

To define the mechanistic aspects of TNAP-mediated periodontal regeneration, we used *Ibsp*$^{-/-}$ OCCM.30 immortalized murine cementoblasts that exhibit reduced mineral formation versus WT cells (Ao et al. 2017). *Alpl* expression was 80% reduced in *Ibsp*$^{-/-}$ versus WT cells at day 1 ($P < 0.01$; Fig. 5A). When compared with media from WT controls, *Ibsp*$^{-/-}$ cells exhibited 40% reduced P_i levels. Addition of 100-µg/mL bIAP increased P_i levels in WT and *Ibsp*$^{-/-}$ cell media by 2- to 3-fold ($P < 0.01$; Fig. 5B). When compared with WT cells, *Ibsp*$^{-/-}$ cells showed less mineralization. Addition of bIAP increased mineralization in WT and *Ibsp*$^{-/-}$ cells; however, mineral deposited by bIAP-treated *Ibsp*$^{-/-}$ lagged that of treated WT cells by day 6 ($P < 0.01$; Fig. 5C).

In addition to contributing to hydroxyapatite crystal growth, P_i acts as a signaling factor for many cells, including cementoblasts (Beck et al. 2000; Rutherford et al. 2006; Chaudhary et al. 2016). Based on increased media P_i concentrations from bIAP treatment, we tested whether inhibiting P_i transport into cells would impair positive effects on mineralization. We employed PFA, a nonspecific low-affinity competitive inhibitor of type II sodium P_i cotransporters (Foster et al. 2006; Addison et al. 2007). A low concentration of 0.1mM PFA was used to reduce potential direct effects of altered P_i on mineral nodule formation, described previously (Villa-Bellosta et al. 2009). Addition of PFA inhibited bIAP-induced increase in mineral nodule formation in WT and *Ibsp*$^{-/-}$ cells, though effects of PFA on *Ibsp*$^{-/-}$ cells were minimal and mineral deposition by WT and *Ibsp*$^{-/-}$ cells treated with bIAP and PFA were equivalent (Fig. 5D). In the presence of bIAP, *Spp1* expression in control and *Ibsp*$^{-/-}$ cells was increased by >20-fold ($P < 0.0001$). PFA inhibited *Spp1* expression in WT and *Ibsp*$^{-/-}$ cells by 55% ($P < 0.001$; Fig. 5E). bIAP increased *Dmp1* expression in WT and *Ibsp*$^{-/-}$ cells by 42- and 10-fold, respectively, as compared with untreated cells ($P < 0.0001$). Phosphate-induced *Dmp1* expression in WT and *Ibsp*$^{-/-}$ cells was inhibited with PFA by ≥50% ($P < 0.001$; Fig. 5F). *Aspn* expression was increased in *Ibsp*$^{-/-}$ cells versus WT cells by 7-fold ($P < 0.001$). bIAP decreased *Aspn* expression in WT and *Ibsp*$^{-/-}$ cells by 50% to 100% ($P < 0.01$), though P_i-induced downregulation of *Aspn* expression was not affected by PFA (Fig. 5G). *Alpl* expression in *Ibsp*$^{-/-}$ cells was significantly decreased with bIAP by 37% ($P < 0.0001$), with a trend in WT cells. There was a trend of

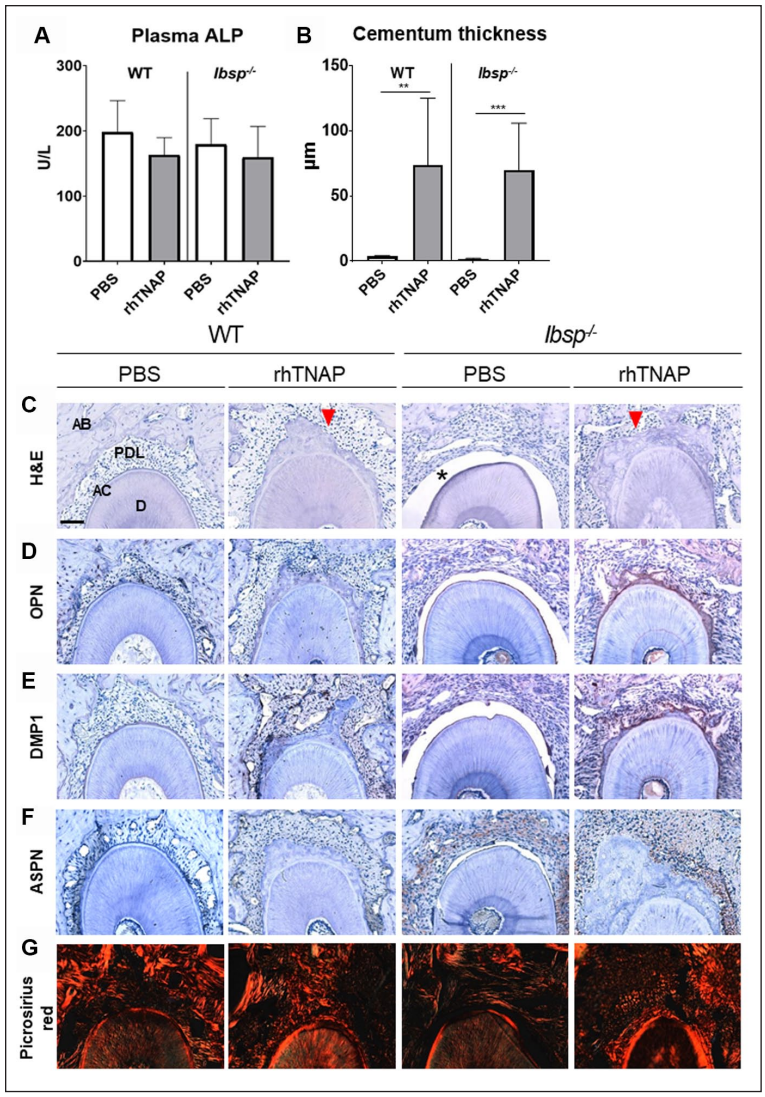

Figure 3. Local delivery of rhTNAP increases regenerated cementum thickness. Fenestration defects were created in 5-wk-old wild type (WT) and *Ibsp*$^{-/-}$ mice, and healing was analyzed at postoperative day 45 (POD 45). (**A**) There were no significant differences in plasma alkaline phosphatase (ALP) levels in vehicle- versus rhTNAP-treated WT and *Ibsp*$^{-/-}$ mice at POD 45 ($n = 6$/group; $P > 0.05$ by independent samples *t* test in pairwise comparisons for each genotype). PBS, phosphate-buffered saline (vehicle). (**B**) When compared with PBS, local delivery of rhTNAP significantly increased cementum thickness in WT and *Ibsp*$^{-/-}$ mice (21- and 42-fold, respectively) by POD 45. ($n = 6$ mice/group; $^{**}P < 0.01$, $^{***}P < 0.001$ by *t* test). Values are presented as mean ± SD. (**C**) Hematoxylin and eosin (H&E) staining reveals lack of acellular cementum (AC) on root dentin (D) and detachment of the periodontal ligament (PDL) from root surfaces (*) in PBS-treated *Ibsp*$^{-/-}$ mice. AB, alveolar bone. rhTNAP promotes AC formation and PDL attachment (arrowhead) in *Ibsp*$^{-/-}$ mice. Thick AC formation (arrowhead) is observed in rhTNAP-treated WT mice. Immunohistochemistry reveals that rhTNAP restores localization of (**D**) osteopontin (OPN) and (**E**) Dentin matrix protein 1 (DMP1) in regenerated AC in *Ibsp*$^{-/-}$ mice, with no apparent difference in rhTNAP- versus PBS-treated WT mice. (**F**) rhTNAP attenuates ASPN localization within the PDL of WT and *Ibsp*$^{-/-}$ mice. (**G**) Local delivery of rhTNAP promoted PDL attachment in *Ibsp*$^{-/-}$ mice, confirmed by picrosirius red staining. Scale bar: 200 µm.

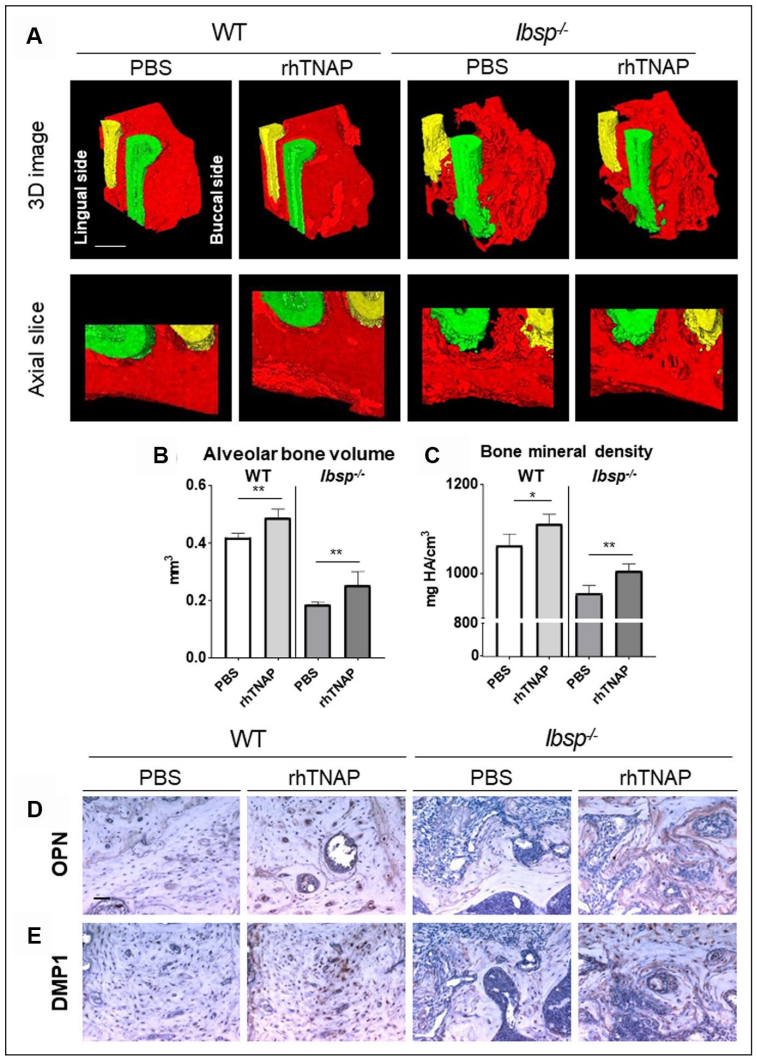

Figure 4. Increased regeneration of alveolar bone with local delivery of rhTNAP. Fenestration defects were created in 5-wk-old wild type (WT) and *Ibsp*$^{-/-}$ mice, and healing was analyzed at postoperative day 45. (**A**) Three-dimensional (3D) micro–computed tomography renderings of first mandibular molar distal (green) and second mesial (yellow) roots and surrounding alveolar bone (AB; red). Scale bar: 500 μm. (**B**) rhTNAP increases regenerated alveolar bone volume by 37% and (**C**) bone mineral density by 5% in *Ibsp*$^{-/-}$ mice ($n = 6$ mice/group; $^{*}P < 0.05$; $^{**}P < 0.01$ by t test). Values are presented as mean ± SD. When compared with phosphate-buffered saline (PBS) vehicle treatment, rhTNAP increases AB volume and mineral density in WT mice by 17% and 5%, respectively. (**D**, **E**) Immunohistochemistry reveals that rhTNAP increases osteopontin (OPN) and dentin matrix protein 1 (DMP1) in regenerated alveolar bone of both WT and *Ibsp*$^{-/-}$ mice. Scale bar: 200 μm.

increased *Alpl* expression with PFA in WT and *Ibsp*$^{-/-}$ cells (Fig. 5H), though PFA did not affect bIAP-induced media P_i concentrations of WT and *Ibsp*$^{-/-}$ (Appendix Fig. 3). These results suggest that bIAP-induced mineralization by WT cells depends more on P_i import (and potential signaling), while bIAP-induced mineralization in *Ibsp*$^{-/-}$ cells may occur through P_i import as well as direct effects on mineralization processes.

Discussion

Accumulative data have revealed that the periodontium, particularly cementum, is sensitive to regulators of P_i/PP_i metabolism (Zweifler et al. 2015; Thumbigere-Math et al. 2018; Chu et al. 2020; Nagasaki et al. 2020). We determined whether pharmacologic modulation of P_i/PP_i through delivery of mineralization-promoting enzyme TNAP could promote cementogenesis using a novel *Ibsp*$^{-/-}$ mouse model of periodontal breakdown. Systemic delivery of TNAP-D_{10} increased plasma ALP levels and restored cementogenesis and periodontal attachment in *Ibsp*$^{-/-}$ mice, confirming that pharmacologic approaches to modulate P_i/PP_i can overcome inherent periodontal defects in *Ibsp*$^{-/-}$ mice. rhTNAP delivery in a periodontal fenestration defect model promoted increased cementum and bone regeneration and restored periodontal attachment in *Ibsp*$^{-/-}$ mice, confirming that increasing local TNAP promotes regeneration in a healing model. Importantly, rhTNAP increased regenerated cementum thickness in WT mice, supporting this as a generalizable approach for periodontal regeneration. Increasing ALP via delivery of bIAP partially rescued mineralization defects in *Ibsp*$^{-/-}$ cementoblasts in vitro and was implicated in direct effects on mineralization and on expression of ECM proteins.

P_i/PP_i Modulation Corrects Dental Development

Extensive literature supports the concept that development and function of periodontal tissues are affected by perturbations in P_i/PP_i metabolism. Inactivating mutations in *ALPL* cause reduced TNAP function, decreased circulating ALP, and increased PP_i levels in the inherited disorder HPP (OMIM#241500, 241510, 146300; Whyte 2016; Bowden and Foster 2019). Dental defects, including acellular cementum hypoplasia, periodontal disease, and premature loss of primary and secondary dentition, are common among individuals with HPP. These periodontal defects are phenocopied in HPP mouse models (McKee et al. 2011; Zweifler et al. 2015; Foster et al. 2017). Evidence for the role played by P_i in the mineralization process is highlighted by inherited hypophosphatemic disorders. X-linked hypophosphatemia (OMIM# 307800) is caused by inactivating mutations in *PHEX* and results in hypophosphatemia associated with skeletal and dental mineralization disorders, including hypomineralized dentin, thin cementum, and poorly mineralized alveolar bone (Biosse Duplan et al. 2017).

Therapies to correct the P_i/PP_i ratio in disorders of phosphate metabolism have shown promising results for periodontal tissues in basic and translational studies. Correction of the P_i/PP_i ratio by addition of P_i improved mineralization in primary PDL and dental pulp cells from patients with HPP (Rodrigues et al. 2012a, 2012b). Enzyme replacement therapy with mineral-targeted TNAP-D_{10} has been effective at correcting prolonging the life span and normalizing skeletal and dental mineralization in HPP mouse models (Millan et al. 2008; McKee et al. 2011; Foster et al. 2012; Whyte 2016). Enzyme replacement therapy has been effective as a first-in-class treatment for patients with HPP, though data analyzing therapeutic effects on dentoalveolar tissues are lacking (Bowden and Foster 2019).

Modulation of P_i/PP_i for Periodontal Regeneration

These collective data suggest that factors modulating P_i/PP_i are candidates to promote periodontal repair and regeneration. Herein, we show that pharmacologic reduction of PP_i levels and concomitant increase of P_i levels effectively promoted cementogenesis. Systemic delivery of a TNAP-D_{10}–encoding lentiviral construct, shown to prolong survival and improve skeletal mineralization in *Alpl*$^{-/-}$ mice (Yamamoto et al. 2011), promoted cementogenesis, retention of periodontal attachment, and maintenance of alveolar bone in *Ibsp*$^{-/-}$ mice that exhibit periodontal breakdown (Foster et al. 2013; Foster et al. 2015). This proof-of-principle experiment provided the first evidence that pharmacologic administration of TNAP could effectively enhance cementogenesis in the face of the mineralization deficiency caused by lack of bone sialoprotein.

An additional key experiment tested the effects of local rhTNAP delivery. Local rhTNAP delivery significantly increased alveolar bone volume and mineral density and promoted cementum regeneration on the root surface in *Ibsp*$^{-/-}$ and WT mice. Furthermore, local rhTNAP delivery induced PDL attachment and restored ECM localization of mineralization markers OPN and DMP1 in *Ibsp*$^{-/-}$ mice. Differences between vehicle-treated and rhTNAP-treated WT mice were not apparent, suggesting that POD 45 may be a "postactive phase" where regeneration has been completed. Previous studies suggest ASPN is an inhibitor of mineralization (Yamada et al. 2007; Kajikawa et al. 2014) with increased expression in PDL of *Ibsp*$^{-/-}$ mice (Ao et al. 2017). Local rhTNAP delivery decreased localization of ASPN in PDL of *Ibsp*$^{-/-}$ mice. These data confirm and extend findings from systemic delivery experiments, supporting local rhTNAP delivery as a viable strategy to promote periodontal regeneration. Benefits of local delivery approaches include a finite promineralization activity focused locally and a lower potential for side effects than systemic delivery. While the concept has not been explored in the context of the

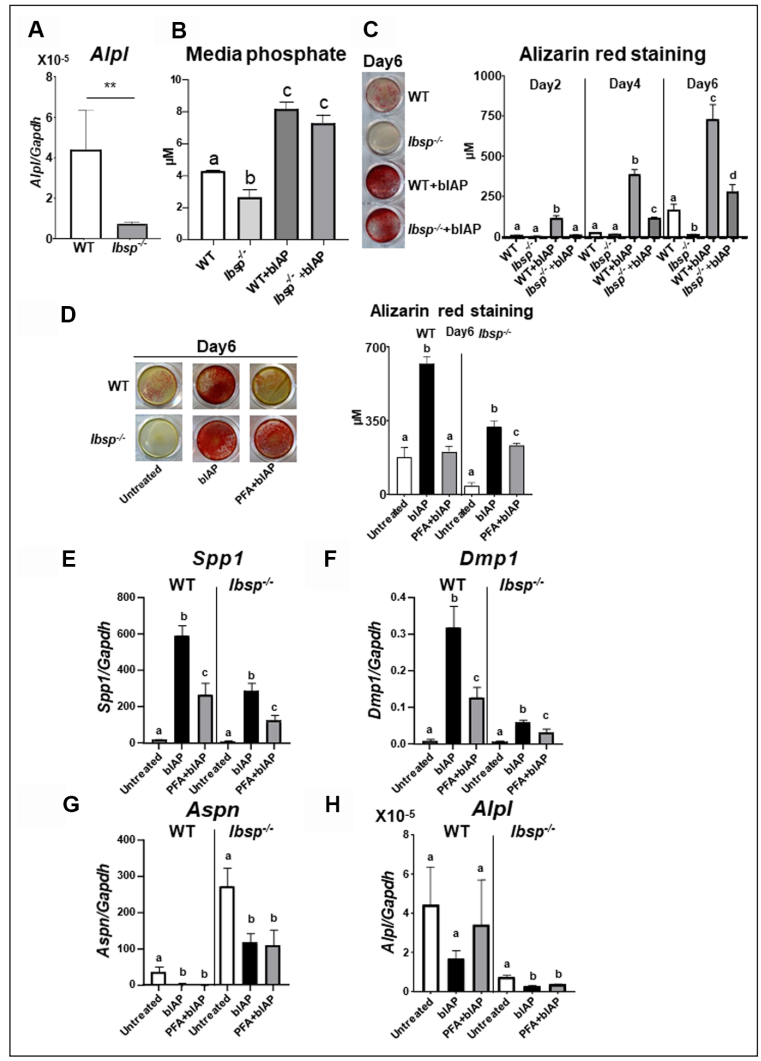

Figure 5. Bovine intestinal alkaline phosphatase (bIAP) increases mineralization in cementoblasts. Wild type (WT) and *Ibsp*$^{-/-}$ OCCM.30 immortalized murine cementoblasts were used to test effects of bIAP on cell expression and mineralization in vitro. (**A**) *Alpl* expression is 80% reduced in *Ibsp*$^{-/-}$ versus WT cells at day 1 (**$P <$ 0.01). (**B**) When compared with media from untreated WT controls, untreated *Ibsp*$^{-/-}$ cells exhibit 40% reduced P_i levels. Addition of 100-μg/mL bIAP increases P_i levels in both WT and *Ibsp*$^{-/-}$ cell media (different letters, $P < 0.01$). (**C**) *Ibsp*$^{-/-}$ cells show less mineralization than do WT cells. Addition of bIAP increases mineralization in WT and *Ibsp*$^{-/-}$ cells. Mineral deposited by bIAP-treated *Ibsp*$^{-/-}$ cells lags that of treated WT cells by day 6 (different letters, $P < 0.01$). (**D**) Addition of 0.1mM phosphonoformic acid (PFA) inhibits bIAP-induced increase in mineral nodule formation in WT and *Ibsp*$^{-/-}$ cells, though effects of PFA on *Ibsp*$^{-/-}$ cells are minimal and mineral deposition by WT and *Ibsp*$^{-/-}$ cells treated with bIAP and PFA is equivalent. (**E**) bIAP increases *Spp1* expression in control and *Ibsp*$^{-/-}$ cells. PFA inhibits *Spp1* expression in WT and *Ibsp*$^{-/-}$ cells by 55% (different letters, $P < 0.001$). (**F**) bIAP increases *Dmp1* expression in WT and *Ibsp*$^{-/-}$ cells versus untreated cells. Phosphate-induced *Dmp1* expression in WT and *Ibsp*$^{-/-}$ cells is partially inhibited by PFA (different letters, $P < 0.001$). (**G**) *Aspn* expression is increased in *Ibsp*$^{-/-}$ cells versus WT cells. bIAP decreases *Aspn* expression in WT and *Ibsp*$^{-/-}$ cells (different letters, $P < 0.01$). P_i-induced downregulation of *Aspn* expression is not affected by PFA. (**H**) *Alpl* expression in *Ibsp*$^{-/-}$ cells was significantly decreased with bIAP by 37% ($P < 0.0001$) with a trend in WT cells. There was a trend of increased *Alpl* expression with PFA in WT and *Ibsp*$^{-/-}$ cells. Values are presented as mean ± SD.

periodontal disease, TNAP and its intestinal analog (intestinal ALP) have anti-inflammatory properties via detoxification of bacterial lipopolysaccharides, adding a potential therapeutic benefit aside from promoting cementum and alveolar bone mineralization (Goldberg et al. 2008; Lalles 2014; Pettengill et al. 2017).

Cell culture experiments revealed that bIAP partially rescued mineralization deficiency in *Ibsp*$^{-/-}$ OCCM.30 cementoblasts in association with increased P_i and altered gene expression, confirming in vivo outcomes. Addition of PFA, a nonspecific competitive inhibitor of type II sodium P_i cotransporters, inhibited bIAP-induced increase mineralization, suggesting that the positive effects of TNAP in vivo may be in part related to its ability to increase local levels of P_i.

These findings show through multiple in vivo and in vitro approaches that pharmacologic modulation of P_i/PP_i metabolism can overcome periodontal breakdown and promote cementum regeneration. Based on limitations of the current models, additional studies focusing on expanded doses, multiple time points, and models incorporating periodontitis and large animals are underway.

Author Contributions

A. Nagasaki, contributed to conception, design, data acquisition, analysis, and interpretation, drafted and critically revised the manuscript; K. Nagasaki, contributed to conception, design, data acquisition, analysis, and interpretation, critically revised the manuscript; B.D. Kear, W.D. Tadesse, contributed to design, data acquisition, and analysis, critically revised the manuscript; V. Thumbigere-Math, contributed to design, data analysis, and interpretation, critically revised the manuscript; J.L. Millán, B.L. Foster, M.J. Somerman, contributed to conception, design, and data interpretation, critically revised the manuscript. All authors gave final approval and agree to be accountable for all aspects of the work.

Acknowledgments

We thank Dr. Davide Randazzo, Dr. Evelyn Ralston, and Aster Kinea (Light Imaging Section, National Institute of Arthritis and Musculoskeletal and Skin Diseases/National Institutes of Health) for assistance in slide scanning and Dr. Vardit Kram (National Institute of Dental and Craniofacial Research/National Institutes of Health) for assistance with micro–computed tomography scanning.

Declaration of Conflicting Interests

The authors declared no potential conflicts of interest with respect to the research, authorship, and/or publication of this article.

Funding

The authors disclosed receipt of the following financial support for the research, authorship, and/or publication of this article: This work was funded by the Japan Society for the Promotion of Science to A. Nagasaki (JSPS Research Fellowship for Japanese Biomedical and Behavioral Researchers at the National Institutes of Health); by the National Institute of Dental and Craniofacial Research/National Institutes of Health to V. Thumbigere-Math (grants R00DE028439 and R03DE029258), B.L. Foster (R03DE028411 and R01DE027639), and J.L. Millán (grant R01DE12889); and by intramural funding from the National Institute of Arthritis and Musculoskeletal and Skin Diseases/National Institutes of Health to M.J. Somerman.

ORCID iDs

A. Nagasaki https://orcid.org/0000-0002-7655-9658
B.L. Foster https://orcid.org/0000-0003-3444-0576

References

Addison WN, Azari F, Sorensen ES, Kaartinen MT, McKee MD. 2007. Pyrophosphate inhibits mineralization of osteoblast cultures by binding to mineral, up-regulating osteopontin, and inhibiting alkaline phosphatase activity. J Biol Chem. 282(21):15872–15883.

Ao M, Chavez MB, Chu EY, Hemstreet KC, Yin Y, Yadav MC, Millan JL, Fisher LW, Goldberg HA, Somerman MJ, et al. 2017. Overlapping functions of bone sialoprotein and pyrophosphate regulators in directing cementogenesis. Bone. 105:134–147.

Beck GR Jr, Zerler B, Moran E. 2000. Phosphate is a specific signal for induction of osteopontin gene expression. Proc Natl Acad Sci U S A. 97(15):8352–8357.

Biosse Duplan M, Coyac BR, Bardet C, Zadikian C, Rothenbuhler A, Kamenicky P, Briot K, Linglart A, Chaussain C. 2017. Phosphate and vitamin d prevent periodontitis in X-linked hypophosphatemia. J Dent Res. 96(4):388–395.

Bowden SA, Foster BL. 2019. Alkaline phosphatase replacement therapy for hypophosphatasia in development and practice. Adv Exp Med Biol. 1148:279–322.

Chaudhary SC, Kuzynski M, Bottini M, Beniash E, Dokland T, Mobley CG, Yadav MC, Poliard A, Kellermann O, Millan JL, et al. 2016. Phosphate induces formation of matrix vesicles during odontoblast-initiated mineralization in vitro. Matrix Biol. 52–54:284–300.

Chu EY, Vo TD, Chavez MB, Nagasaki A, Mertz EL, Nociti FH, Aitken SF, Kavanagh D, Zimmerman K, Li X, et al. 2020. Genetic and pharmacologic modulation of cementogenesis via pyrophosphate regulators. Bone. 136:115329.

Dutra EH, Chen IP, Reichenberger EJ. 2013. Dental abnormalities in a mouse model for craniometaphyseal dysplasia. J Dent Res. 92(2):173–179.

Eke PI, Zhang X, Lu H, Wei L, Thornton-Evans G, Greenlund KJ, Holt JB, Croft JB. 2016. Predicting periodontitis at state and local levels in the United States. J Dent Res. 95(5):515–522.

Foster BL, Ao M, Willoughby C, Soenjaya Y, Holm E, Lukashova L, Tran AB, Wimer HF, Zerfas PM, Nociti FH Jr, et al. 2015. Mineralization defects in cementum and craniofacial bone from loss of bone sialoprotein. Bone. 78:150–164.

Foster BL, Kuss P, Yadav MC, Kolli TN, Narisawa S, Lukashova L, Cory E, Sah RL, Somerman MJ, Millan JL. 2017. Conditional Alpl ablation phenocopies dental defects of hypophosphatasia. J Dent Res. 96(1):81–91.

Foster BL, Nagatomo KJ, Nociti FH Jr, Fong H, Dunn D, Tran AB, Wang W, Narisawa S, Millan JL, Somerman MJ. 2012. Central role of pyrophosphate in acellular cementum formation. PLoS One. 7(6):e38393.

Foster BL, Nociti FH Jr, Swanson EC, Matsa-Dunn D, Berry JE, Cupp CJ, Zhang P, Somerman MJ. 2006. Regulation of cementoblast gene expression by inorganic phosphate in vitro. Calcif Tissue Int. 78(2):103–112.

Foster BL, Popowics TE, Fong HK, Somerman MJ. 2007. Advances in defining regulators of cementum development and periodontal regeneration. Curr Top Dev Biol. 78:47–126.

Foster BL, Soenjaya Y, Nociti FH Jr, Holm E, Zerfas PM, Wimer HF, Holdsworth DW, Aubin JE, Hunter GK, Goldberg HA, et al. 2013. Deficiency in acellular cementum and periodontal attachment in BSP null mice. J Dent Res. 92(2):166–172.

Goldberg RF, Austen WG Jr, Zhang X, Munene G, Mostafa G, Biswas S, McCormack M, Eberlin KR, Nguyen JT, Tatlidede HS, et al. 2008. Intestinal alkaline phosphatase is a gut mucosal defense factor maintained by enteral nutrition. Proc Natl Acad Sci U S A. 105(9):3551–3556.

Ho AM, Johnson MD, Kingsley DM. 2000. Role of the mouse ANK gene in control of tissue calcification and arthritis. Science. 289(5477):265–270.

Kajikawa T, Yamada S, Tauchi T, Awata T, Yamaba S, Fujihara C, Murakami S. 2014. Inhibitory effects of PLAP-1/asporin on periodontal ligament cells. J Dent Res. 93(4):400–405.

King GN, King N, Cruchley AT, Wozney JM, Hughes FJ. 1997. Recombinant human bone morphogenetic protein-2 promotes wound healing in rat periodontal fenestration defects. J Dent Res. 76(8):1460–1470.

Lalles JP. 2014. Intestinal alkaline phosphatase: novel functions and protective effects. Nutr Rev. 72(2):82–94.

McKee MD, Nakano Y, Masica DL, Gray JJ, Lemire I, Heft R, Whyte MP, Crine P, Millan JL. 2011. Enzyme replacement therapy prevents dental defects in a model of hypophosphatasia. J Dent Res. 90(4):470–476.

Millan JL. 2006. Mammalian alkaline phosphatases: from biology to applications in medicine and biotechnology. Weinheim (Germany): Wiley-VCH Verlag GmbH & Co. p. 1–322.

Millan JL, Narisawa S, Lemire I, Loisel TP, Boileau G, Leonard P, Gramatikova S, Terkeltaub R, Camacho NP, McKee MD, et al. 2008. Enzyme replacement therapy for murine hypophosphatasia. J Bone Miner Res. 23(6):777–787.

Nagasaki A, Nagasaki K, Chu EY, Kear BD, Tadesse WD, Ferebee SE, Li L, Foster BL, Somerman MJ. Ablation of pyrophosphate regulators promotes periodontal regeneration. J Dent Res [epub ahead of print 24 Dec 2020] in press. doi:10.1177/0022034520981854

Osathanon T, Giachelli CM, Somerman MJ. 2009. Immobilization of alkaline phosphatase on microporous nanofibrous fibrin scaffolds for bone tissue engineering. Biomaterials. 30(27):4513–4521.

Pettengill M, Matute JD, Tresenriter M, Hibbert J, Burgner D, Richmond P, Millan JL, Ozonoff A, Strunk T, Currie A, et al. 2017. Human alkaline phosphatase dephosphorylates microbial products and is elevated in preterm neonates with a history of late-onset sepsis. PLoS One. 12(4):e0175936.

Rodrigues TL, Foster BL, Silverio KG, Martins L, Casati MZ, Sallum EA, Somerman MJ, Nociti FH Jr. 2012a. Correction of hypophosphatasia-associated mineralization deficiencies in vitro by phosphate/pyrophosphate modulation in periodontal ligament cells. J Periodontol. 83(5):653–663.

Rodrigues TL, Foster BL, Silverio KG, Martins L, Casati MZ, Sallum EA, Somerman MJ, Nociti FH Jr. 2012b. Hypophosphatasia-associated deficiencies in mineralization and gene expression in cultured dental pulp cells obtained from human teeth. J Endod. 38(7):907–912.

Rodrigues TL, Nagatomo KJ, Foster BL, Nociti FH, Somerman MJ. 2011. Modulation of phosphate/pyrophosphate metabolism to regenerate the periodontium: a novel in vivo approach. J Periodontol. 82(12):1757–1766.

Rutherford RB, Foster BL, Bammler T, Beyer RP, Sato S, Somerman MJ. 2006. Extracellular phosphate alters cementoblast gene expression. J Dent Res. 85(6):505–509.

Rutsch F, Ruf N, Vaingankar S, Toliat MR, Suk A, Hohne W, Schauer G, Lehmann M, Roscioli T, Schnabel D, et al. 2003. Mutations in ENPP1 are associated with "idiopathic" infantile arterial calcification. Nat Genet. 34(4):379–381.

Sallum EA, Ribeiro FV, Ruiz KS, Sallum AW. 2019. Experimental and clinical studies on regenerative periodontal therapy. Periodontol 2000. 79(1):22–55.

Szeri F, Lundkvist S, Donnelly S, Engelke UFH, Rhee K, Williams CJ, Sundberg JP, Wevers RA, Tomlinson RE, Jansen RS, et al. 2020. The membrane protein ANKH is crucial for bone mechanical performance by mediating cellular export of citrate and ATP. PLoS Genet. 16(7):e1008884.

Thumbigere-Math V, Alqadi A, Chalmers NI, Chavez MB, Chu EY, Collins MT, Ferreira CR, FitzGerald K, Gafni RI, Gahl WA, et al. 2018. Hypercementosis associated with ENPP1 mutations and gaci. J Dent Res. 97(4):432–441.

Villa-Bellosta R, Ravera S, Sorribas V, Stange G, Levi M, Murer H, Biber J, Forster IC. 2009. The Na+-Pi cotransporter PiT-2 (SLC20A2) is expressed in the apical membrane of rat renal proximal tubules and regulated by dietary Pi. Am J Physiol Renal Physiol. 296(4):F691–F699.

Vora SR, Camci ED, Cox TC. 2016. Postnatal ontogeny of the cranial base and craniofacial skeleton in male C57BL/6J mice: a reference standard for quantitative analysis. Front Physiol. 6:417.

Whyte MP. 2016. Hypophosphatasia—aetiology, nosology, pathogenesis, diagnosis and treatment. Nat Rev Endocrinol. 12(4):233–246.

Yamada S, Tomoeda M, Ozawa Y, Yoneda S, Terashima Y, Ikezawa K, Ikegawa S, Saito M, Toyosawa S, Murakami S. 2007. PLAP-1/asporin, a novel negative regulator of periodontal ligament mineralization. J Biol Chem. 282(32):23070–23080.

Yamamoto S, Orimo H, Matsumoto T, Iijima O, Narisawa S, Maeda T, Millan JL, Shimada T. 2011. Prolonged survival and phenotypic correction of Akp2(−/−) hypophosphatasia mice by lentiviral gene therapy. J Bone Miner Res. 26(1):135–142.

Zweifler LE, Patel MK, Nociti FH Jr, Wimer HF, Millan JL, Somerman MJ, Foster BL. 2015. Counter-regulatory phosphatases TNAP and NPP1 temporally regulate tooth root cementogenesis. Int J Oral Sci. 7(1):27–41.